THE JOURNAL OF PHYSICAL CHEMISTRY B

ARTICLE

pubs.acs.org/JPCB

Kinetics of Coupling Water and Cryoprotectant Transport across Cell Membranes and Applications to Cryopreservation

Lindong Weng, Weizhong Li,* Cong Chen, and Jianguo Zuo

Key Laboratory of Ocean Energy Utilization and Energy Conservation of Ministry of Education, Dalian University of Technology, Dalian, Liaoning 116024, China

ABSTRACT:

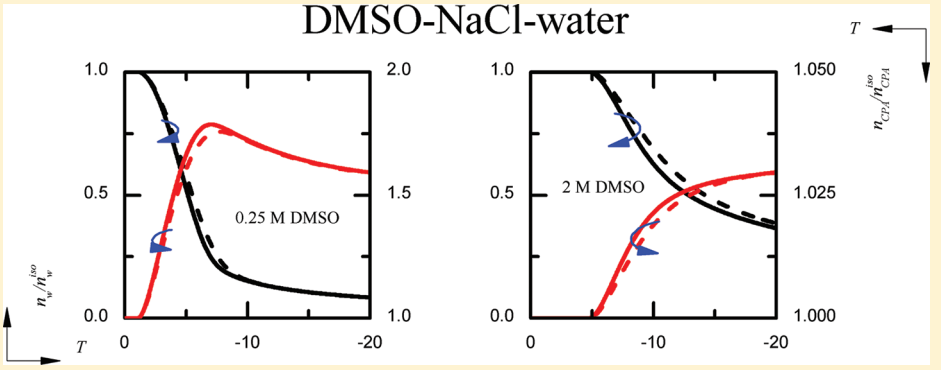

Thermodynamic and kinetic models can provide a wealth of information on the physical response of living cells and tissues experiencing cryopreservation procedures. Both isothermal and nonisothermal models have been proposed so far, accompanied by experimental verification and cryoapplications. But the cryoprotective solution is usually assumed to be dilute and ideal in the models proposed in the literature. Additionally, few nonisothermal models are able to couple the transmembrane transport of water and cryoprotectant during cooling and warming of cells. To overcome these limitations, this study develops a whole new set of equations that can quantify the cotransport of water and cryoprotectant across cell membranes in the nondilute and nonideal solution during the freezing and thawing protocols. The new models proposed here can be simplified into ones consistent with the classic models if some specific assumptions are included. For cryobiological practice, they are applied to predict the volumetric change for imprinting control region (ICR) mouse spermatozoa and human corneal keratocytes in the freezing protocol. The new models can determine the intracellular concentration of cryoprotectant more precisely than others by abandoning the assumptions such as dilute and ideal solutions and nonpermeability of membranes to cryoprotectant. Further, the findings in this study will offer new insights into the physical response of cells undergoing cryopreservation.

1. INTRODUCTION

The field of cryobiology has progressed as a fertile ground for new discoveries with important applications in both cryopreservation and cryosurgery. One of the most striking discoveries is that Polge et al.[1] revealed the cryoprotective property of glycerol when cryopreserving human spermatozoa. Nowadays, the addition and removal of cryoprotective agents (CPAs) have become indispensible procedures to the efforts of preserving biomaterials at low temperatures. A complete process of cryopreservation commonly includes, in sequence, the addition of permeable CPAs into biological cells, the freezing protocol (e.g., multistep cooling and vitrification), the long-term storage in liquid nitrogen, the thawing protocol, and the removal of permeable CPAs out of cells.

During most of the above-mentioned procedures, the transmembrane transport of water and permeable CPAs occurs. As for the cooling of cells, the outside solution is concentrated as the formation of extracellular ice proceeds. The larger osmotic pressure in the outer space than in the inner space, as a result, drives the efflux of intracellular water. Another example is that, when permeable CPAs are provided into cells before the freezing protocol, the efflux and subsequent influx of water occur in order to ease the unbalanced CPA chemical potential across cell membranes.

For clarifying the intricate details about the mass transfer across cell membranes occurring during the above procedures, many thermodynamic and kinetic models were proposed, and their experimental verification was conducted.[2] According to our observation, the major models available in the literature are summarized in Tables 1 and 2. Table 1 generally classifies these models into two categories. They are (1) the isothermal model that determines the water and CPA movement across membranes

Received: June 9, 2011
Revised: September 29, 2011
Published: October 31, 2011

Table 1. A Summary of Various Theoretical Models in Cryobiology

	simple water transport	water and permeable CPAs cotransport
isothermal		models proposed by Jacobs and Stewart[3,4] Kedem and Katchalsky;[5] Katkov;[10] Elliott et al.[9,19]
nonisothermal	models proposed by Mazur;[11] Karlsson et al.;[12] Fahy;[13] Elliott et al.;[9,19] Saenz et al.;[15] Weng et al.[14]	

Table 2. Scopes of Application of Various Theoretical Models in Cryobiology

	Dilute solution	Nondilute solution
ideal solution	models proposed by Jacobs and Stewart;[3,4] Kedem and Katchalsky;[5] Katkov;[10] Mazur;[11] Karlsson et al.[12]	
nonideal solution	models proposed by Fahy;[13] Saenz et al.;[15] Weng et al.[14]	models proposed by Elliott et al.[9,19]

during the addition and removal of permeable CPAs at a constant temperature and (2) the nonisothermal one that calculates the water loss of cells subjected to cooling and warming. Then, Table 2 compares the different application conditions of these models. Note that the models developed for the nonideal solution can be simplified into ideal ones; those established for the nondilute solution are suitable for the dilute one in a reduced form as well.

1.1. The Isothermal Model. In 1932, Jacobs and Stewart[3,4] proposed a model for predicting the volumetric change of cells when they are exposed to hypotonic or hypertonic surroundings containing a permeable solute without temperature change. Their model consisted of two differential equations and was modified into the modern two-parameter (2-P) model by later researchers. Jacobs and Stewart and other like-minded researchers, however, did not include the solute−solvent interaction when the solute and solvent were cotransported through a common channel in cell membranes. In 1958, Kedem and Katchalsky[5] developed the well-known K−K model using Onsager's irreversible thermodynamic approach[6,7] as shown by eqs 1−3.[8] Their theory filled up the above-mentioned insufficiency by introducing the reflection coefficient σ.[9] In the K−K model, σ was used to evaluate the interaction between the solute and the solvent when a common channel was shared by them. $\sigma = 0$ is indicative of the pronounced dependence of the solute flow on the volume flow.[5] $\sigma = 1 - (P_S\bar{v}_{CPA}/RTL_P)$, on the other hand, implies that the solute and the solvent cross cell membranes through independent pathways.[8] That way, the modern 2-P and K−K models calculate the total volume flow dV_c/dt identically.

$$\frac{dV_c}{dt} = -L_P ART[(\pi^e_{salt} - \pi^i_{salt}) + \sigma(\pi^e_{CPA} - \pi^i_{CPA})] \quad (1)$$

$$\frac{dn_{CPA}}{dt} = (1-\sigma)\frac{\pi^e_{CPA} + \pi^i_{CPA}}{2}\frac{dV_c}{dt} + P_S A(\pi^e_{CPA} - \pi^i_{CPA}) \quad (2)$$

$$0 \le \sigma \le 1 - \frac{P_S\bar{v}_{CPA}}{RTL_P} \quad (3)$$

where V_c is the cell volume, n_{CPA} is the mole content of the intracellular CPA, t is the time, L_P is the hydraulic conductivity, P_S is the membrane CPA permeability, A is the surface area of the cell, $\bar{v}_{CPA}$ is the partial molar volume of CPA, T is the temperature, R is the universal gas constant, and π is the osmolality with the superscripts denoting the extra- (e) and intracellular (i) space.

Both the reviews by Kleinhans[8] and Elmoazzen et al.[9] provide excellent entry points into the modern 2-P and K−K models. As discussed in the literature,[8,9] the introduction of σ is still debatable since there are few instances of significant cotransport of water and CPAs in the field of cryobiology. Katkov,[10] for example, believed that there was no mutual "dragging" of the solute and the solvent in the membrane, thereby developing a new model for multisolute systems on the basis of the modern 2-P model.

In spite of the long-running dispute about σ, the fact is well acknowledged that both modern 2-P and K−K models and their other improved formalisms are subject to a dilute and ideal solution. Although it was stated that the concentration should be osmolarity,[3,4] Jacobs and Stewart[9] directly used molarity in their study. Similarly, Kedem and Katchalsky conducted the derivation of their pertinent equations by assuming that the solutions were dilute and ideal, even if they stated that the real solution could be evaluated by the activity factor.[5] Osmolality and osmolarity are often used interchangeably for a dilute solution,[9] while for an ideal solution $\pi = \upsilon_s \cdot m_s$ with the osmotic coefficient $\phi \equiv 1$ (υ_s is the dissociation constant for solute and m_s the molality in M).

1.2. The Nonisothermal Model. Mazur,[11] in 1963, initiated the quantitative prediction of the water content inside living cells experiencing the freezing protocol. It is the first-ever nonisothermal model in the field of cryobiology. His pioneering theory was derived from the difference in the chemical potential of water, and he obtained the original formalism (i.e., eq 4) by using Raoult's law.[11] However, several assumptions were unavoidably made, which were explained at the end of his paper.[11] Cell membranes, for example, were assumed to be permeable only to water. Also he assumed the extracellular solution and the protoplasm were dilute and ideal. What's more, the molar heat of fusion ΔH_f was considered to be constant and independent of T.

$$\frac{dV_c}{dT} = \frac{L_P ART}{B\bar{v}_w}\left[\frac{\Delta H_f}{R}\left(\frac{1}{T_R} - \frac{1}{T}\right) - \ln\frac{(V_c - V_b)}{(V_c - V_b) + \upsilon_{salt}n_{salt}\bar{v}_w}\right] \quad (4)$$

where B is the cooling rate, n_{salt} is the mole content of the intracellular salt, υ_{salt} is the dissociation constant for salt, $\bar{v}_w$ is the partial molar volume of water, T_R is the reference temperature, and V_b is the osmotically inactive volume.

The popularity of the Mazur model as the foundation for the quantitative analysis in cryobiology has been reflected in the successive presence of many improved ones. For instance, in the work by Karlsson et al.,[12] the Mazur model was expanded into a new one in which the volume of the intracellular CPA was taken into account as shown by eq 5. One can notice that the Karlsson model also inherited the assumptions included in the Mazur model.

$$\frac{dV_c}{dT} = \frac{L_p ART}{B\overline{v}_w}\left[\frac{\Delta H_f}{R}\left(\frac{1}{T_R}-\frac{1}{T}\right) - \ln\frac{(V_c - V_b - \overline{v}_{CPA}n_{CPA})}{(V_c - V_b - \overline{v}_{CPA}n_{CPA}) + \overline{v}_w(v_{salt}n_{salt} + n_{CPA})}\right] \quad (5)$$

1.3. Improvement of Models for Nondilute, Nonideal Solutions. It is clear that both isothermal and nonisothermal models mentioned above focus primarily on dilute and ideal solutions. The assumption of a dilute and ideal solution can often be met under physiological conditions, but it is hardly appropriate in most cryobiological cases.[9] Therefore, further efforts were devoted to exclude this major assumption. Fahy[13] calculated the water content inside living cells that experienced linear cooling profiles in a dilute but nonideal solution. The factor *f* was used in his model to represent the nonideality of the solution, but it failed to be readily available in most phase diagrams.[14] Recently, Saenz et al.[15] developed the model for the cell dehydration in the nonideal solution during the freezing protocol. In their model, the Debye−Hückel theory was applied to evaluate the nonideality induced by the strong electrolyte character of sodium chloride (NaCl). Weng et al.[14] introduced the osmotic coefficient ϕ to evaluate the nonideality of CPA−NaCl−water mixtures, thereby proposing a new model to predict the osmotic water flow across cell membranes in nonideal solutions during cooling and warming.

The above evaluations of nonideality can only deal with the chemical potential of water, but they are ineligible for the chemical potential of solute. This is one of the reasons why all of them were integrated into nonisothermal models in which the chemical potential of solute was unnecessary. A more general improvement, however, was proposed and applied in recent work by Elliott and her co-workers.[9,16−21]

Elliott et al.[19] expressed the chemical potential of water in a real solution as polynomials in terms of the mole fraction and molality, respectively, on the basis of the Gibbs free energy and the regular solution theory. Then, the osmolality of the real solution was obtained through the osmotic virial equation and used in the nonisothermal model. In the recent work by Ross-Rodriguez et al.,[20,21] for example, the multisolute osmotic virial expression was integrated into the water transport equation of the modern 2-P model in which both two-step and graded cooling profiles were included. The main purpose of their work was to calculate the supercooling of the intracellular space and contrast the simulation result with membrane integrity measured by experiments with the hope of explaining high recovery of TF-1 cells after cryostorage in the absence of traditional CPAs such as dimethyl sulfoxide (DMSO). Since no CPAs were added into cryomedia in the study of Ross-Rodriguez et al.,[20,21] no work was done to determine the CPA permeation during the cooling of cells. Although the permeation of CPAs such as DMSO and propylene glycol (PG) was examined by Mukherjee et al.[22] based on the nonideal thermodynamics,[9,19] the specific case of interest was isothermal (i.e., at 22 °C). On the other hand, Elmoazzen et al.[9] reanalyzed the volumetric change of human corneal epithelial cells on addition of various concentrations of DMSO at 13 °C by including the transmembrane transport of solute. In their study, the chemical potential of solute in the real solution was represented explicitly and used to establish their nondilute solute transport equation, which was an extension of the work by Elliott et al.[19] In effect, the formalisms reported by Elmoazzen et al.[9] have not yet been further developed to cover cooling and warming of living cells, to the best of our knowledge.

From the above brief review of the main thermodynamic and kinetic models in cryobiology, one can notice that one issue remains to be addressed. Namely, studies have not yet been carried out so far to couple the transport of water and permeable CPAs of cells subjected to the freezing and thawing protocols, particularly in cryomedia that are neither nondilute nor nonideal. One of the challenges, in our opinion, should be the difficulty in determining the changing concentration of the extracellular solution. However, this challenge can be undertaken through two different approaches depending on the model assumption, which will be unraveled in section 2. Additionally, the conventional nonisothermal models such as the Mazur and Karlsson ones typically assume that cell membranes are solely permeable to water. This assumption, on the contrary, is necessarily excluded in the isothermal models. Therefore, there exists a contradiction that has yet bto be resolved.

The present study develops a new set of nonisothermal equations that are able to calculate the cotransport of water and permeable CPAs across cell membranes when living cells are cooled and warmed in nondilute and nonideal solutions. Also, the new models can certainly resolve the above contradiction. The versatility of our models is reflected by the fact that they are applicable to both isothermal conditions and dilute and ideal solutions through certain simplifications.

This paper is organized in the following way. First, the derivations of our new models are presented for the dilute and ideal solution and for the nondilute and nonideal one, respectively. Then, we evaluate the deviation of the simulation result caused by ignoring the permeable CPA transport and calculate the content of the intracellular CPA of cells during cooling and warming. In the end, the new nonisothermal models are applied to the cryopreservation of imprinting control region (ICR) mouse spermatozoa and human corneal keratocytes, respectively.

2. THEORY

The new set of equations in this study is developed by assuming water and permeable CPAs cross membranes through independent pathways. This is justified because studies on membrane channels to date have revealed few instances of significant cotransport of water and solute.[8,9] Specifically, the discovery and characterization of aquaporins[23−25] have revolutionized our understanding of the transmembrane transport of water. Aquaporins (i.e., water channels) selectively conduct water molecules into and out of the cell while preventing the passage of ions and other solutes. Moreover, the derivation of our equations considers a ternary mixture of CPA, NaCl, and water for illustrative clarity. But our new models can be applied to more complicated systems by some necessary extensions.

2.1. The Transmembrane Transport of Water and Permeable CPAs in a Dilute and Ideal Solution. The theory of osmosis and diffusion lays the foundation for calculating the

transport of water and permeable CPAs across cell membranes. The case of interest is freezing and thawing cells dynamically in a dilute and ideal CPA−NaCl−water mixture.

2.1.1. The Dilute and Ideal Water Transport Equation. The water flux across cell membranes is driven by the difference between the chemical potential of water outside μ_w^e and that inside μ_w^i. Equation 6 can calculate the mole content of the intracellular water n_w as a function of time t in minutes.[9]

$$\frac{dn_w}{dt} = k_w A(\mu_w^e - \mu_w^i) \tag{6}$$

where k_w is the water permeability coefficient in $mol^2 \cdot min^{-1} \cdot atm^{-1} \cdot \mu m^{-5}$ and A the area of the plasma membrane in μm^2.

The chemical potential of water μ_w in $J \cdot mol^{-1}$ in an ideal solution can be written as[26]

$$\mu_w = \mu_w^0 + RT \ln(x_w) \tag{7}$$

where μ_w^0 is the chemical potential of pure water at the same temperature T and pressure P as the solution, and x_w is the mole fraction of water in either the extra- or intracellular space.

For an ideal solution consisting of n solutes and water, $\ln(x_w)$ can be correlated with the solution molality m_s according to the following equation:[26]

$$\ln(x_w) = -M_w \sum_{s=1}^{n} \upsilon_s m_s \tag{8}$$

where M_w is the molar mass of water in $kg \cdot mol^{-1}$. $\upsilon_s = 1$ for nonelectrolyte CPAs such as glycerol and DMSO and $\upsilon_s = 2$ for NaCl due to the existence of Na^+ and Cl^-.

Therefore, eq 6 can be rearranged into the following one that can determine the volumetric change rate of the intracellular water according to m_s.

$$\frac{dV_w}{dt} = -M_w \bar{v}_w k_w ART\left(\sum \upsilon_s m_s^e - \sum \upsilon_s m_s^i\right) \tag{9}$$

where V_w is the volume of the intracellular water in μm^3.

When the cell is cooled and warmed dynamically at a rate B (= dT/dt) in $°C \cdot min^{-1}$, eq 9 would take the form

$$\frac{dV_w}{dT} = -M_w \bar{v}_w k_w ART\left(\sum \upsilon_s m_s^e - \sum \upsilon_s m_s^i\right)/B \tag{10}$$

The coefficient k_w can be converted into a commonly used form (i.e., hydraulic conductivity L_P in $\mu m \cdot atm^{-1} \cdot min^{-1}$) according to $L_P = M_w \bar{v}_w k_w / \rho_w$ where ρ_w is the density of water. Then, eq 10 would take the form

$$\frac{dV_w}{dT} = -L_P ART\left(\sum \upsilon_s m_s^e - \sum \upsilon_s m_s^i\right)/B \tag{11}$$

where $m_s = n_s/V_w$ for the sake of dimensional uniform.

Since the osmolality of an ideal solution $\pi = \Sigma\, \upsilon_s m_s$ in Osm, one can obtain

$$\frac{dV_w}{dT} = -L_P ART(\pi^e - \pi^i)/B \tag{12}$$

Equation 12 indicates that the intracellular water can freely flow across cell membranes in the direction of lower to higher osmolality, which is referred to as osmosis.

2.1.2. The Dilute and Ideal CPA Transport Equation. Fick's first law of diffusion states that

$$\frac{dn_{CPA}}{dt} = P_S A(c_{CPA}^e - c_{CPA}^i) \tag{13}$$

where c_{CPA}^e and c_{CPA}^i are the molarity of the extra- and intracellular solute, respectively, and P_S is the membrane CPA permeability in $\mu m \cdot min^{-1}$. c_{CPA} and m_{CPA} can be used interchangeably for a dilute solution,[9] thereby transmuting eq 13 into the following form:

$$\frac{dn_{CPA}}{dt} = P_S A(m_{CPA}^e - m_{CPA}^i) \tag{14}$$

where $m_{CPA}^i = n_{CPA}/V_w$ for the dimensional uniform.

When the cell is cooled and warmed dynamically at a rate B, eq 14 takes the form

$$\frac{dn_{CPA}}{dT} = P_S A(m_{CPA}^e - m_{CPA}^i)/B \tag{15}$$

Equation 15 suggests that the permeable CPA can enter the cell as long as the extracellular solution is progressively concentrated due to the extracellular ice growth. Hence, the total volumetric change can be given by

$$\frac{dV_c}{dT} = \frac{dV_w}{dT} + \bar{v}_{CPA}\frac{dn_{CPA}}{dT} \tag{16}$$

Both L_P and P_S are temperature-dependent, which can be expressed as

$$L_P = L_{pg} \exp\left[\frac{E_{Lp}}{R}\left(\frac{1}{T_0} - \frac{1}{T}\right)\right] \tag{17}$$

$$P_S = P_{sg} \exp\left[\frac{E_{Ps}}{R}\left(\frac{1}{T_0} - \frac{1}{T}\right)\right] \tag{18}$$

where L_{pg} and P_{sg} are the permeability parameters at the reference temperature T_0 (i.e., 273.15 K), and E_{Lp} and E_{Ps} are the activation energies for L_P and P_S in $kcal \cdot mol^{-1}$, respectively.

The osmolality of the extracellular solution π^e would take the form[16]

$$\pi^e = \frac{T_m^0 - T_m}{RT_m M_w/(s_w^{0L} - s_w^{0s})} \tag{19}$$

where s_w^{0L} and s_w^{0S} are the entropy per mole of pure water in the liquid and the solid phase, respectively, T_m^0 is the freezing point of pure water, and T_m is the freezing point of the extracellular solution, which is equal to T since the extracellular solution is assumed to be in equilibrium with ice.

As mentioned earlier, $\pi = \upsilon_{salt} m_{salt} + \upsilon_{CPA} m_{CPA}$, so that one can calculate m_{salt}^e and m_{CPA}^e as follows:

$$m_{salt}^e = \frac{\pi^e}{\upsilon_{salt} + \upsilon_{CPA} R' \dfrac{M_{salt}}{M_{CPA}}} \tag{20}$$

$$m_{CPA}^e = R' \frac{\pi^e}{\upsilon_{salt}\dfrac{M_{CPA}}{M_{salt}} + \upsilon_{CPA} R'} \tag{21}$$

where M_{salt} and M_{CPA} are the molar mass of salt and CPA in $kg \cdot mol^{-1}$, respectively, and R' is the mass ratio of CPA and

NaCl. Given that the outside space is relatively infinite compared with the cell volume, R' can be considered as a constant.

Equations 12 and 15 can determine the contents of water and permeable CPA in cells during the freezing and thawing protocols with the assumption of a dilute and ideal solution. And two parameters (i.e., L_P and P_S) are used to characterize the membrane permeabilities. Hence, in this study, eqs 12 and 15 and their subsidiary equations are termed the dilute and ideal nonisothermal 2-P model as a whole.

2.1.3. Simplification of the Dilute and Ideal Nonisothermal 2-P Model. When cells are subjected to the addition and removal of CPAs at a constant T (i.e., $B \equiv 0$), eqs 12 and 15 will take the forms

$$\frac{dV_w}{dt} = -L_P ART(\pi^e - \pi^i) \tag{22}$$

$$\frac{dn_{CPA}}{dt} = P_S A(m^e_{CPA} - m^i_{CPA}) \tag{23}$$

The fact is eqs 22 and 23 represent the well-known modern 2-P model including only isothermal equations with the assumption of a dilute and ideal solution.

If cell membranes are assumed to be ideal semipermeable (i.e., $P_S = 0$), on the other hand, eq 12 would be solely solved and able to describe the transmembrane transport of water identically with the Karlsson model as discussed in section 3.1.

2.2. The Transmembrane Transport of Water and Permeable CPAs in a Nondilute and Nonideal Solution. The principle is again that the mass transfer is driven by the difference between the extra- and intracellular chemical potentials. Given that the activity of the solute in a nonideal solution cannot be conveniently calculated, a recently developed expression for the chemical potential of the solute μ_s is employed here.[9] Meanwhile, the corresponding expression for μ_w is also used to achieve a thermodynamic consistence.

2.2.1. The Nondilute and Nonideal Water and Permeable CPA Transport Equations. In this study, the chemical potentials of water and CPA, μ_w and μ_{CPA}, in a real CPA−NaCl−water mixture are derived from the work by Elliott and her coworkers,[9,17,19] as shown by eqs 24 and 25. In their work, the Gibbs free energy of a real solution was separated into the ideal part and the excess one. For the excess part of the Gibbs free energy, the interchange energy ω and the osmotic virial coefficient B were introduced.

$$\mu_w = \mu^0_w - RT\left[(1 - x_w) + B_{CPA}x_{CPA}{}^2 + B_{salt}x_{salt}{}^2 + (B_{CPA} + B_{salt})x_{CPA}x_{salt}\right] \tag{24}$$

$$\mu_{CPA} = \mu^0_{CPA} + RT\left[\ln(x_{CPA}) + \left(\frac{1}{2} - B_{CPA}\right)x_w(1 - x_{CPA}) - \left(\frac{1}{2} - B_{salt}\right)x_w x_{salt}\right] \tag{25}$$

where μ^0_w and μ^0_{CPA} are the chemical potentials of pure water and pure CPA, respectively, at the same T and P as the solution.[26] x_w, x_{CPA}, and x_{salt} are the mole fractions of water, CPA, and salt in the ternary mixture, respectively. B_{CPA} and B_{salt} are the osmotic virial coefficients for CPA and salt based on a virial expansion in mole fraction up to the second order. For example, B_{CPA} is equal to 4.716 for DMSO, 2.950 for glycerol, and 3.415 for PG, and B_{salt} is equal to 2.759 for NaCl.[9]

Thus, the two mole fluxes (i.e., dn_w/dt and dn_{CPA}/dt) take the following forms:

$$\frac{dn_w}{dt} = -k_w ART\left[(1 - x^e_w) + B_{CPA}x^e_{CPA}{}^2 + B_{salt}x^e_{salt}{}^2 + (B_{CPA} + B_{salt})x^e_{CPA}x^e_{salt} - (1 - x^i_w) - B_{CPA}x^i_{CPA}{}^2 - B_{salt}x^i_{salt}{}^2 - (B_{CPA} + B_{salt})x^i_{CPA}x^i_{salt}\right] \tag{26}$$

$$\frac{dn_{CPA}}{dt} = k_{CPA}ART\left[\ln(x^e_{CPA}) + \left(\frac{1}{2} - B_{CPA}\right)x^e_w(1 - x^e_{CPA}) - \left(\frac{1}{2} - B_{salt}\right)x^e_w x^e_{salt} - \ln(x^i_{CPA}) - \left(\frac{1}{2} - B_{CPA}\right)x^i_w(1 - x^i_{CPA}) + \left(\frac{1}{2} - B_{salt}\right)x^i_w x^i_{salt}\right] \tag{27}$$

where k_{CPA} is the CPA permeability coefficient in $mol^2 \cdot \mu m^{-5} \cdot min^{-1} \cdot atm^{-1}$.

Considering the freezing and thawing protocols with a rate B, eqs 26 and 27 would take the forms

$$\frac{dn_w}{dT} = -k_w ART\left[(1 - x^e_w) + B_{CPA}x^e_{CPA}{}^2 + B_{salt}x^e_{salt}{}^2 + (B_{CPA} + B_{salt})x^e_{CPA}x^e_{salt} - (1 - x^i_w) - B_{CPA}x^i_{CPA}{}^2 - B_{salt}x^i_{salt}{}^2 - (B_{CPA} + B_{salt})x^i_{CPA}x^i_{salt}\right]/B \tag{28}$$

$$\frac{dn_{CPA}}{dT} = k_{CPA}ART\left[\ln(x^e_{CPA}) + \left(\frac{1}{2} - B_{CPA}\right)x^e_w(1 - x^e_{CPA}) - \left(\frac{1}{2} - B_{salt}\right)x^e_w x^e_{salt} - \ln(x^i_{CPA}) - \left(\frac{1}{2} - B_{CPA}\right)x^i_w(1 - x^i_{CPA}) + \left(\frac{1}{2} - B_{salt}\right)x^i_w x^i_{salt}\right]/B \tag{29}$$

As with L_P and P_S, k_w and k_{CPA} are also temperature-dependent as described by eqs 30 and 31.

$$k_w = k_{wg}\exp\left[\frac{E_{kw}}{R}\left(\frac{1}{T_0} - \frac{1}{T}\right)\right] \tag{30}$$

$$k_{CPA} = k_{CPAg}\exp\left[\frac{E_{kCPA}}{R}\left(\frac{1}{T_0} - \frac{1}{T}\right)\right] \tag{31}$$

where k_{wg} and k_{CPAg} are the water and CPA permeability parameters at T_0, respectively, and E_{kw} and E_{kCPA} are the activation energies for k_w and k_{CPA} in $kcal \cdot mol^{-1}$, respectively.

2.2.2. Determination of the Extracellular Mole Fraction of Water, CPA, and Salt. For a nondilute and nonideal CPA−NaCl−water mixture, x^e_w, x^e_{CPA}, and x^e_{salt} can be determined on the basis of its ternary phase diagram by assuming that the ice is in equilibrium with the residual solution. Nowadays, many phase diagrams of CPA−NaCl−water mixtures are available. Moreover, the synthesis of binary phase diagrams into ternary ones has been validified,[27−29] which can enrich the current database of phase diagrams. The determination of x^e_w, x^e_{CPA}, and x^e_{salt} in the nondilute and nonideal DMSO−NaCl−water mixture is illustrated as follows. The calculations for other more complicated mixtures can be similarly done.

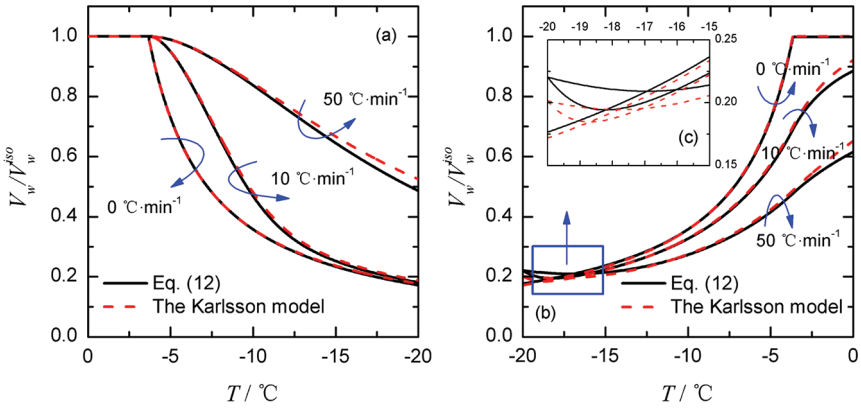

Figure 1. Normalized water content V_w/V_w^{iso} in EBVT lymphocyte at temperature T when cooled at 0, 10, and 50 °C·min^{-1} (a) and warmed at 0 °C·min^{-1}after an equilibrium cooling and at 10 and 50 °C·min^{-1} after cooled at 20 °C•min^{-1} (b). Note that inset c is a partial enlargement of panel b.

T_m of the DMSO−NaCl−water mixture as a function of its total solute concentration S (g in 100 g solution) and the mass ratio of DMSO and NaCl R' takes the form[30]

$$T_m = (-0.6 + 0.17\tan^{-1} R')\cdot S + [\tan^{-1}(R'/2)/132 - 0.001]\cdot S^2 - 0.00045\cdot S^2 + 273.15 \quad (32)$$

S can be determined by reversely solving eq 32, and x^e_{CPA} and x^e_{salt} at a given T_m are given by the following equations:

$$x^e_{CPA} = [v_{CPA}\cdot S\cdot R'/(R'+1)]/M_{CPA}/[v_{CPA}\cdot S\cdot R'/(R'+1)]/M_{CPA} + [v_{salt}\cdot S/(R'+1)]/M_{salt} + (100-S)/M_w \quad (33)$$

$$x^e_{salt} = [v_{salt}\cdot S/(R'+1)]/M_{salt}[v_{CPA}\cdot S\cdot R'/(R'+1)]/M_{CPA} + [v_{salt}\cdot S/(R'+1)]/M_{salt} + (100-S)/M_w \quad (34)$$

$$x^e_w = 1 - x^e_{CPA} - x^e_{salt} \quad (35)$$

Equations 28 and 29 are developed to couple the transport of water and permeable CPAs of cells in a nondilute and nonideal solution. k_w and k_{CPA} are used to characterize the membrane permeabilities. Therefore, eqs 28 and 29 and their subsidiary equations are termed the nondilute and nonideal nonisothermal 2-P model in this study.

2.2.3. Simplification of the Nondilute and Nonideal Nonisothermal 2-P Model. The nondilute and nonideal nonisothermal 2-P model can be simplified into one for a dilute and ideal solution if the excess part of the Gibbs free energy is neglected. In other words, B_{CPA} and B_{salt} in eqs 28 and 29 are set to zero to yield

$$\frac{dn_w}{dT} = -k_w ART[(1-x^e_w) - (1-x^i_w)]/B \quad (36)$$

$$\frac{dn_{CPA}}{dT} = k_{CPA} ART[\ln(x^e_{CPA}) - \ln(x^i_{CPA})]/B \quad (37)$$

where P_S and k_{CPA} have the relation $P_S = k_{CPA}RT/[(c^e_{CPA} + c^i_{CPA})/2]$ but it can only hold for a dilute and ideal solution.[9]

3. RESULTS AND DISCUSSION

Investigations of the new models are carried out in the following ways. In subsection 3.1, the equality between eq 12 and the Karlsson model is verified under the limitation of an ideal semipermeable membrane. In subsection 3.2, we analyze the differences in the simulation results induced by ignoring the permeable CPA transport during the freezing and thawing protocols. In subsection 3.3, the nonisothermal 2-P models are applied to determine the physical response of ICR mouse spermatozoa and human corneal keratocytes subjected to a dynamic freezing protocol. This subsection also evaluates the differences between the results from the dilute and ideal nonisothermal 2-P model and those from the nondilute and nonideal nonisothermal one.

Table 3. Cellular Characteristics of the Hypothetical Spherical Cell

parameter	value	unit	parameter	value	unit
L_{pg}	0.15	μm·atm^{-1}·min^{-1}	D_{iso}	10	μm
E_{Lp}	12	kcal·mol^{-1}	V_b/V_{iso}	0.3	1
P_{sg}	5	μm·min^{-1}	C^0_{CPA} (glycerol)	1	mol·L^{-1}
E_{Ps}	10	kcal·mol^{-1}	B	20	°C·min^{-1}

3.1. Equality between eq 12 and the Karlsson Model. Equation 12 is theoretically consistent with the Karlsson model, as stated in our previous research.[14] The current study, on the other hand, indicates that eq 12 and the Karlsson model can produce identical results under the same conditions, where the Epstein−Barr virus-transformed (EBVT) lymphocyte is cooled and warmed in equilibrium (i.e., 0 °C·min^{-1}) and dynamic (i.e., 10 and 50 °C·min^{-1}) manners respectively. The cell is initially exposed to a ternary mixture of glycerol, NaCl, and water with 1.5 M glycerol. The geometric and membrane characteristics of the EBVT lymphocyte were reported by Devireddy et al.[31] In their original work, L_P was measured in the absence of any CPAs.[31] In this study, we continue using the original value of L_P since there are no interactions between water and glycerol in the membrane. The water content in the EBVT lymphocyte as a function of the subzero temperature T (in °C) is calculated based on eq 12 and the Karlsson model, respectively. The normalized water content V_w/V_w^{iso} in the cell during cooling and warming is shown in Figure 1 in which V_w^{iso} is the isotonic content of the intracellular water.

The temperature dependence of ΔH_f is taken into consideration in this study when solving the Karlsson model. ΔH_f was assumed to be constant (i.e., 333.35 J·g^{-1}) in previous studies[11,12] but ΔH_f is actually temperature dependent, as pointed

dx.doi.org/10.1021/jp2054348 |J. Phys. Chem. B 2011, 115, 14721–14731

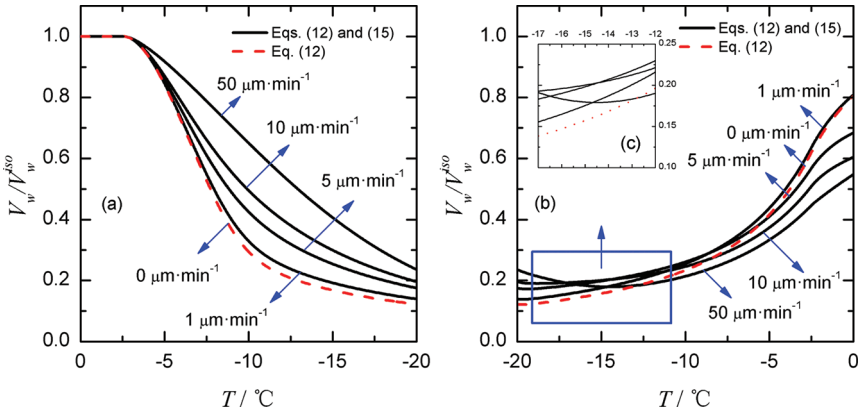

Figure 2. Normalized water content V_w/V_w^{iso} at temperature T of hypothetical cells with various membrane glycerol permeabilities P_{sg} when cooled at 20 °C·min^{-1} (a) and warmed at 20 °C·min^{-1} afterward (b). Note that inset c is a partial enlargement of panel b.

out by Mazur.[11] In this study, the relationship between ΔH_f and T (in °C) takes the form[32]

$$\Delta H_f = 333.35 - \int_{Tm}^{0} (c_w - c_i)\, dT \quad (38)$$

where c_w and c_i are the specific heat capacities of water and ice, respectively, in J·g^{-1}·°C^{-1}.

The values of c_w and c_i as a function of T over a range of 0 to −40 °C are obtained by fitting experimental data[33,34] available to the polynomial representations, respectively. Hence, we obtain[35]

$$c_w = 4.287 + 0.031 \cdot T + 0.004 \cdot T^2 + 1.890 \times 10^{-4} \cdot T^3 + 3.261 \times 10^{-6} \cdot T^4 \quad (39)$$

$$c_i = 2.109 + 0.008 \cdot T + 2.592 \times 10^{-6} \cdot T^2 \quad (40)$$

As shown in Figure 1, differences between the results of eq 12 and those of the Karlsson model are negligible. The slight differences are due to different variables used in these two formalisms such as ΔH_f which is not included in eq 12. The quantitatively same curves given by these two formalisms under the same conditions can prove their equality as a whole.

3.2. Effects of the Permeable CPA Transport on the Physical Response of Cells during Cooling and Warming. Our new nonisothermal models can resolve the underlying contradiction between the modern 2-P and Mazur or Karlsson models by regarding cell membranes to be permeable to both water and penetrating CPAs, as stated earlier. This subsection quantifies the simple water transport and the coupling transport of water and a permeable CPA, respectively. The result of the former case is calculated solely with eq 12 while that of the latter case is obtained by combinedly solving eqs 12 and 15. Thus, the differences between these two cases are simply induced by the CPA permeation and can be determined.

In order to evaluate the effects of the CPA transport, this study introduces a hypothetical spherical cell, the characteristics of which are listed in Table 3. D_{iso} is the isotonic diameter of the cell, V_{iso} is the isotonic cellular volume, and c_{CPA}^0 the initial molality of glycerol as the permeable CPA in this subsection.

It is expected that P_{sg} be the most significant factor that affects the differences between the above-mentioned two cases. Therefore, this study calculates V_w/V_w^{iso} in hypothetical cells with various P_{sg} (i.e., 0, 1, 5, 10, and 50 μm·min^{-1}) as a function of T in the first place. The results have been depicted in Figure 2 where P_{sg} = 0 μm·min^{-1} indicates that cell membranes are impermeable to any solutes.

As seen in Figure 2a, the curve $V_w/V_w^{iso} \sim T$ for P_{sg} = 0 μm·min^{-1} is the lowest among all the presented ones. Without the assistance of the glycerol permeation, the unbalanced water chemical potential across cell membranes can be alleviated only by the outflow of intracellular water. On the contrary, when glycerol is permitted to enter the cell, both the efflux of water and the influx of glycerol can ease the unbalance of the osmotic pressure. In the latter case, the cell will lose less water to achieve the balance compared with the former case. Furthermore, the assistance of the glycerol permeation will become more obvious if P_{sg} increases. This expectation can be proved in Figure 2a by the fact that a larger P_{sg} produces a gentler $V_w/V_w^{iso} \sim T$. For example, at −10.1 °C, the difference between the curves for P_{sg} = 0 μm·min^{-1} and for P_{sg} = 1 μm·min^{-1} arrives at the highest level (i.e., 0.035), whereas that between the curves for P_{sg} = 0 μm·min^{-1} and for P_{sg} = 50 μm·min^{-1} is 0.356, a 10-fold enlargement with a 50-fold increase in P_{sg}.

The situation in Figure 2b tends to be complicated owing to the different starting points of the warming curves. It is noticed that for P_{sg} = 50 μm·min^{-1} there is a noticeable "U" shape at the beginning of the curve. The U shape in the initial part of the warming curve is caused by a temporary larger π^e than π^i given that the equilibrium of mass transfer has not been achieved until the end of the cooling protocol.[14] In addition, one can find that the value of V_w/V_w^{iso} in the warming protocol is always smaller than that in the cooling protocol at the same temperature. The reason for such a difference has been explained in our previous study.[14]

It is speculated that a smaller L_{pg} can affect the simulation result the same way as a larger P_{sg}. This is mainly because a smaller L_{pg} means a weaker advantage over the same P_{sg}, which is equivalent to a larger P_{sg} with the same L_{pg}. Such a speculation is clearly proved in Figure 3. In detail, at −7.8 °C the difference between the curves for L_{pg} = 0 μm·atm^{-1}·min^{-1} and for L_{pg} = 0.3 μm·atm^{-1}·min^{-1} reaches the maximum value of 0.081. However, the largest difference between the curves for L_{pg} = 0 μm·atm^{-1}·min^{-1} and for L_{pg} = 0.05 μm·atm^{-1}·min^{-1} is 0.239 at −18.2 °C.

As indicated by eqs 17 and 18, a smaller E_{Ps} and a larger P_{sg} can produce a larger P_S at a given T than other cases. So do a smaller E_{Lp} and a larger L_{pg}. Therefore, one can easily expect the trends

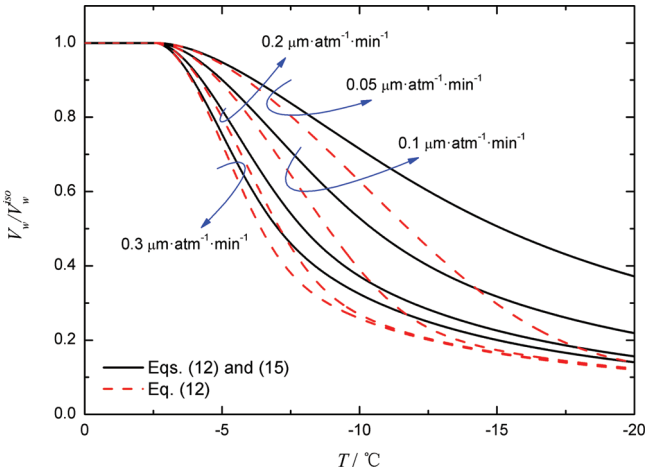

Figure 3. Normalized water content V_w/V_w^{iso} at temperature T of hypothetical cells with various hydraulic conductivities L_{pg} when cooled at 20 °C·min^{-1}.

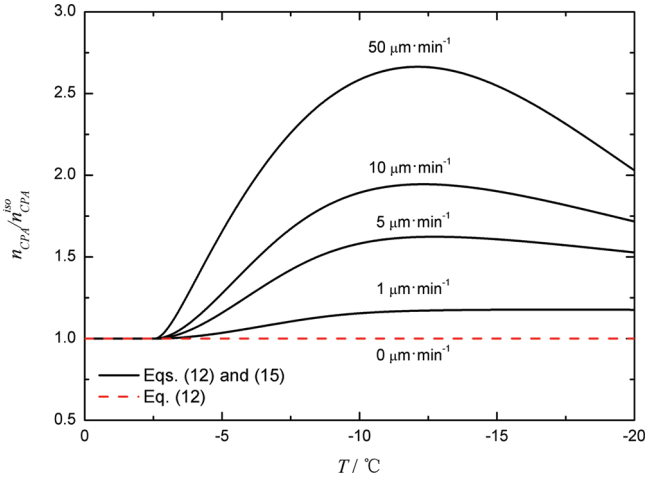

Figure 4. Normalized glycerol content n_{CPA}/n_{CPA}^{iso} at temperature T of hypothetical cells with various membrane glycerol permeabilities P_{sg} during the freezing protocol at 20 °C·min^{-1}.

of $V_w/V_w^{iso} \sim T$ for different E_{Ps} and E_{Lp} according to the results shown in Figures 2 and 3. Moreover, our study has also investigated the simulation results by varying c_{CPA}^0 and D_{iso}, respectively. However, they cannot obviously affect the deviation induced by ignoring the glycerol permeation.

The contents of intracellular CPAs and salts are attention-attracting quantities in cryobiology since they are the indicator of the inside supercooling and the "solute injury". One of the most significant novelties of our new models is to real-time trace the change of these quantities. The quantitative relation between n_{CPA}/n_{CPA}^{iso} and T and that between $m_{CPA}^{i(e)}$ and T have been presented in Figures 4 and 5, respectively. Figure 4 indicates that the amount of glycerol inside the hypothetical cell increases as the extracellular ice grows. Then, glycerol will flow out of the cell after the initial inflow. For P_{sg} = 50 μm·min^{-1}, the value of n_{CPA}/n_{CPA}^{iso} arrives at the peak of 2.66 at −12.2 °C and then falls to 2.03 at −20 °C. This phenomenon can be explained by virtue of the results in Figure 5.

We specify four stages in Figure 5 to fully understand the changing surroundings inside the cell with a decreasing T. Note

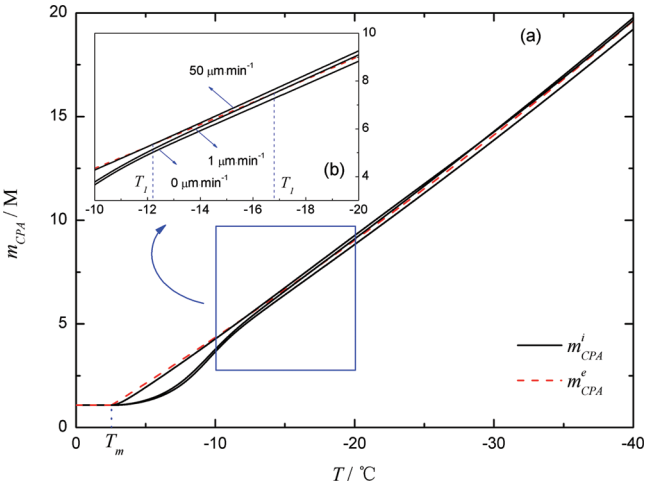

Figure 5. Intra- and extracellular glycerol molalities $m_{CPA}^{i(e)}$ at temperature T of hypothetical cells with various membrane glycerol permeabilities P_{sg} during the freezing protocol at 20 °C·min^{-1}.

that the differences between curves $m_{CPA}^e \sim T$ and $m_{CPA}^i \sim T$ are slight because the initial concentrations of glycerol and NaCl are small, and the temperature range is extended to −40 °C by ignoring the eutectic formation.

(1) The balance of the osmotic pressure across cell membranes can be established if the addition of glycerol is completed. When the extracellular ice is absent (i.e., $T \geq T_m$), $m_{CPA}^e = m_{CPA}^i$ and $m_{salt}^e = m_{salt}^i$ hold.

(2) When $T_1 < T < T_m$, the extracellular ice appears so that the external solution begins to be concentrated. Note that the supercooling of the inside medium is neglected for simplification. As a result, $m_{CPA}^e > m_{CPA}^i$ and $m_{salt}^e > m_{salt}^i$ hold, which can trigger the influx of glycerol and the efflux of water. Since there are two processes, both of which can increase the molality of the intracellular glycerol, $m_{CPA}^i = m_{CPA}^e$ can be achieved earlier than $\pi^i = \pi^e$ or $m_{salt}^e = m_{salt}^i$. Besides, a larger P_{sg} means a stronger effect of the glycerol inflow on the increase in m_{CPA}^i. Thus, for P_{sg} = 50 μm·min^{-1} m_{CPA}^i is equal to m_{CPA}^e at −12.2 °C, while T_1 = −16.8 °C for P_{sg} = 1 μm·min^{-1}.

(3) At $T = T_1$ $m_{CPA}^e = m_{CPA}^i$ holds, which means the inflow of glycerol stops. But the cellular water loss will continue due to $m_{salt}^e > m_{salt}^i$.

(4) As the freezing protocol proceeds (i.e., $T < T_1$), the continuing water loss will result in $m_{CPA}^i > m_{CPA}^e$, which is able to reverse the direction of the glycerol penetration. This is why the amount of the intracellular glycerol decreases in the later stage. Hence, there exist two opposite processes in which m_{CPA}^i can be increased and decreased, respectively. In other words, the overall change of m_{CPA}^i will depend on the competition between these two processes, and such a competition is affected by c_{CPA}^0, P_S, and L_P. In the case of this study, it is clear that m_{CPA}^i finally approaches m_{CPA}^e at a very low temperature.

Equations 12 and 15 indicate that the equilibrium of mass transfer is based on the separate equalities of $m_{CPA}^e = m_{CPA}^i$ and $m_{salt}^e = m_{salt}^i$. However, these equalities may not be achieved at the same temperature or even may not hold at all. In other words, when permeable CPAs and water can cross cell membranes simultaneously, equilibrium is not bound to happen with a given

dx.doi.org/10.1021/jp2054348 |J. Phys. Chem. B 2011, 115, 14721–14731

Table 4. Temperature Dependence of Membrane Water and Glycerol Permeabilities of ICR Mouse Spermatozoa

	K−K model				modern 2-P model	
T (°C)	L_p (μm·atm^{-1}·min^{-1})	P_s (μm·min^{-1})	σ	σ_{NI}	L_p (μm·atm^{-1}·min^{-1})	P_s (μm·min^{-1})
22	0.38	22	0.84	0.83	0.424	20.036
14	0.17	17	0.68	0.69	0.182	16.586
9	0.16	9	0.78	0.82	0.171	9.231
4	0.18	13	0.76	0.77	0.193	12.729
1.5	0.08	4	0.84	0.84	0.085	3.991
−2	0.10	7	0.76	0.78	0.106	7.036

temperature range. Like the case in this study, the cotransport of water and glycerol cannot be fully equilibrated until −20 °C.

3.3. Cryobiological Applications of the Nonisothermal 2-P Models. A majority of theoretical models in cryobiology are employed to predict the physical response of living cells subjected to cryopreservation protocols. Thus, the dilute and ideal nonisothermal 2-P model is applied to predict the volumetric change of ICR mouse spermatozoa when cooled at 5 °C·min^{-1} in a glycerol−NaCl−water mixture according to available data on their membrane permeabilities.[36] The nondilute and nonideal nonisothermal 2-P model, on the other hand, is used to calculate the content of water and CPAs in human corneal keratocytes[37,38] in DMSO−NaCl−water and PG−NaCl−water mixtures, respectively, during the freezing protocol at 5 °C·min^{-1}.

3.3.1. Applications of the Dilute and Ideal Nonisothermal 2-P Model. The characteristics of membrane water and glycerol permeabilities of ICR mouse spermatozoa were determined by Phelps et al.[36] based on the K−K model. Since the current study assumes that no common channels are shared by water and CPAs, eqs 12 and 15 exclude σ, which is necessary in the K−K model. Hence, this study converts L_p, P_s, and σ in the K−K model into L_p and P_s in the modern 2-P model as presented in Table 4. By fitting the values of L_p and P_s in the modern 2-P model at different temperatures to eqs 17 and 18, one can obtain that L_{pg} = 0.1066 μm·atm^{-1}·min^{-1}, E_{Lp} = 8.905 kcal·mol^{-1}, P_{sg} = 8.305 μm·min^{-1} and E_{Ps} = 6.498 kcal·mol^{-1}. In Table 4, it is clear that σ and σ_{NI} have similar values at the same temperature, which proves that water and glycerol pass membranes of ICR mouse spermatozoa through independent channels.

Figure 6 illustrates the volumetric response V_c/V_c^{iso} of ICR mouse spermatozoa subjected to a 5 °C·min^{-1} cooling in solutions of 0.135 and 0.54 M glycerol. Devireddy and his coworkers[39] reported the experimental results of V_c/V_c^{iso} of ICR mouse spermatozoa in such a case. An acceptable agreement can be observed between the prediction results from eqs 12 and 15 and the experimental results.[39] The slight differences between the simulation results and the experimental ones may come from the different developmental stages of ICR mouse spermatozoa in the experiments of Phelps et al.[36] and Devireddy et al.[39] The usage of different culture solutions may contribute to these differences as well.

The volumetric change of the cell is mainly affected by the change of the intracellular water since the solution is dilute and the change in the glycerol content is not very significant. After glycerol is loaded into cells, there is less water in the cell exposed to the 0.54 M solution than in the cell exposed to the 0.135 M solution. As a result, the cell will have less losable water if it is surrounded by a more concentrated solution. This is one of the

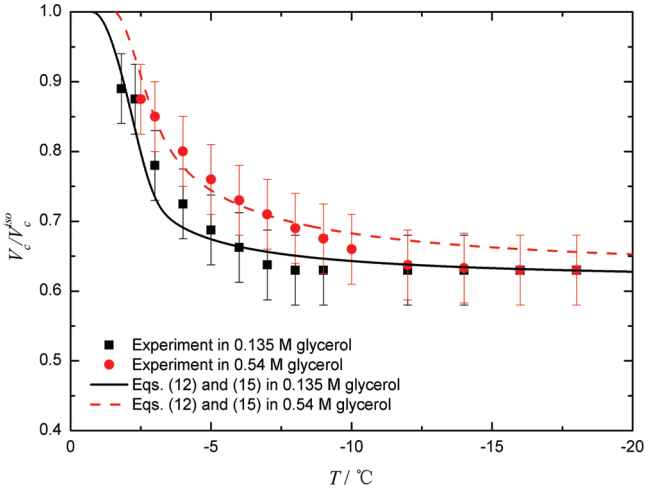

Figure 6. Volumetric response V_c/V_c^{iso} as a function of temperature T of ICR mouse spermatozoa after exposure to a solution of 0.135 or 0.54 M glycerol during a cooling at 5 °C·min^{-1}.

reasons why the volumetric change in spermatozoa exposed to the 0.135 M solution is more dramatic than that exposed to 0.54 M at a given T. Moreover, the lag of the extracellular ice formation in the 0.54 M solution compared with that in the 0.135 M solution also results in less water loss at the same T in the former solution.

3.3.2. Applications of the Nondilute and Nonideal Nonisothermal 2-P Model. The characteristics of membrane water, DMSO, and PG permeabilities of human corneal keratocytes were determined by Ebertz et al.[37,38] using the K−K model. L_p, P_s and σ in the K−K model are converted into k_w and k_{CPA} in eqs 26 and 27, as presented in Tables 5 and 6. We fit the values of k_w and k_{CPA} at different temperatures to eqs 30 and 31. As a result, it is obtained that k_{wg} = 2.71 × 10^{-28} mol^2·μm^{-5}·min^{-1}·atm^{-1}; E_{kw}= 14.16 kcal·mol^{-1}; k_{CPAg}= 4.79 × 10^{-32} mol^2·μm^{-5}·min^{-1}·atm^{-1}; E_{kcpa}= 17.03 kcal·mol^{-1} for membrane water and DMSO permeabilities and k_{wg} = 2.54 × 10^{-28} mol^2·μm^{-5}·min^{-1}·atm^{-1}; E_{kw}= 15.24 kcal·mol^{-1}; k_{CPAg}= 4.77 × 10^{-32} mol^2·μm^{-5}·min^{-1}·atm^{-1}; E_{kcpa}= 17.48 kcal·mol^{-1} for membrane water and PG permeabilities.

The normalized water and DMSO contents n_w/n_w^{iso} and n_{CPA}/n_{CPA}^{iso} in human corneal keratocytes as a function of T are calculated with eqs 28 and 29 and eqs 36 and 37, respectively. Figure 7 shows the prediction results when the cells are cooled at 5 °C·min^{-1} after initial exposure to DMSO−NaCl−water mixtures with 0.25 and 2 M DMSO, respectively.

Figure 7 clearly illustrates the differences between the results from eqs 28 and 29 and those from eqs 36 and 37. Concentration

dx.doi.org/10.1021/jp2054348 |J. Phys. Chem. B 2011, 115, 14721–14731

Table 5. Characteristics of Membrane Permeability of Human Corneal Keratocytes for Water and DMSO at Various T

T (°C)	L_p (μm·atm^{-1}·min^{-1})	P_s (μm·min^{-1})	σ	k_w (mol^2·μm^{-5}·min^{-1}·atm^{-1})	k_{CPA} (mol^2·μm^{-5}·min^{-1}·atm^{-1})
4	0.09	1.99	0.89	3.14×10^{-28}	6.37×10^{-32}
13	0.35	4.27	0.50	1.17×10^{-27}	2.66×10^{-31}
22	0.53	9.76	0.65	2.04×10^{-27}	4.54×10^{-31}
37	1.51	35.74	0.48	5.35×10^{-27}	1.94×10^{-30}

Table 6. Characteristics of Membrane Permeability of Human Corneal Keratocytes for Water and PG at Various T

T (°C)	L_p (μm·atm^{-1}·min^{-1})	P_s (μm·min^{-1})	σ	k_w (mol^2·μm^{-5}·min^{-1}·atm^{-1})	k_{CPA} (mol^2·μm^{-5}·min^{-1}·atm^{-1})
4	0.09	2.15	0.93	3.31×10^{-28}	6.69×10^{-32}
13	0.31	4.28	0.52	1.07×10^{-27}	2.50×10^{-31}
22	0.56	11.40	0.66	2.19×10^{-27}	5.12×10^{-31}
37	1.83	39.44	0.48	6.63×10^{-27}	2.12×10^{-30}

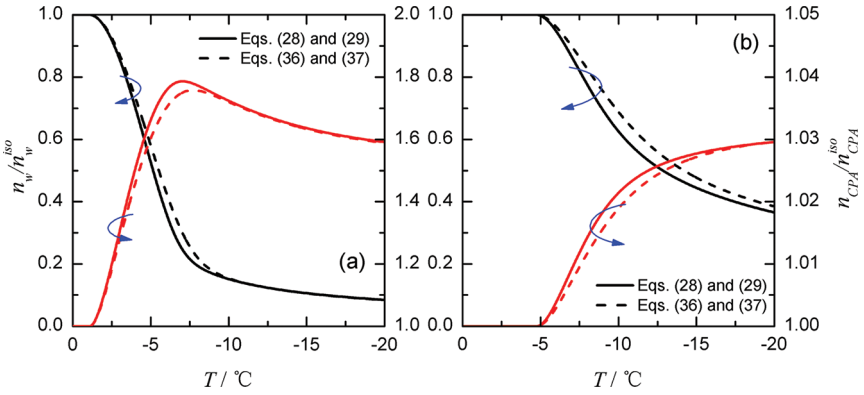

Figure 7. Normalized water and DMSO contents n_w/n_w^{iso} and n_{CPA}/n_{CPA}^{iso} in human corneal keratocytes as a function of temperature T after exposure to DMSO−NaCl−water mixtures of 0.25 M (a) or 2 M (b) DMSO during a cooling at 5 °C·min^{-1}.

is considered to be the most important factor to evaluate how dilute and ideal the solution is. Therefore, as seen in this figure, such differences are enlarged as the solution molality rises from 0.25 to 2 M. It is also found that the differences will become less noticeable when the transport of water and DMSO approaches equilibrium.

One can also observe that n_w/n_w^{iso} given by eqs 36 and 37 is larger than that given by eqs 28 and 29 at a given T. The case is opposite in terms of n_{CPA}/n_{CPA}^{iso}. By ignoring the minimal effect of NaCl in eqs 28 and 36, the driving force for the water flux is $(x_w^i - x_w^e) + B_{CPA}(x_{CPA}^e - x_{CPA}^i)$ in the nondilute and nonideal solution and $x_w^i - x_w^e$ in the dilute and ideal solution, respectively. Since $(x_{CPA}^e)^2 - (x_{CPA}^i)^2 > 0$, the driving force for the water flux in the nonideal and nondilute solution is greater than that in the dilute and ideal solution. In other words, the cell in the nondilute and nonideal solution will lose more water than in the dilute and ideal solution. This is why n_w/n_w^{iso} given by eqs 36 and 37 is larger than that given by eqs 28 and 29 at a given T.

Similarly, by ignoring the minimal effect of NaCl in eqs 29 and 37, the driving force for the CPA flux is $\ln x_{CPA}^e - \ln x_{CPA}^i + (1/2 - B_{CPA})\cdot(x_w^{e\,2} - x_w^{i\,2})$ in the nondilute and nonideal solution and $\ln x_{CPA}^e - \ln x_{CPA}^i$ in the dilute and ideal solution. Since $(1/2 - B_{CPA})(x_w^{e\,2} - x_w^{i\,2})$ is greater than 0, the driving force for the CPA flux in the nondilute and nonideal solution is greater than that in the dilute and ideal solution. This is why n_{CPA}/n_{CPA}^{iso} given by eqs 36 and 37 is smaller than that given by eqs 28 and 29 at a given T. As the transport approaches equilibrium, these differences will be hardly noticed in that the total amount of the losable water is the same in both cases.

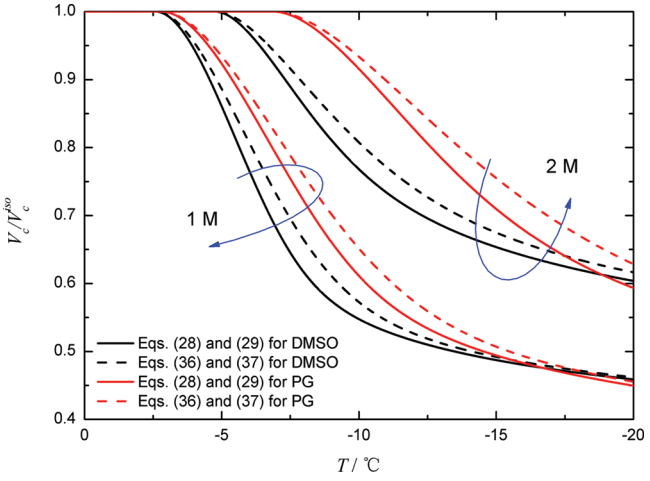

Figure 8. Volumetric response V_c/V_c^{iso} as a function of temperature T of human corneal keratocytes after being exposed to CPA−NaCl−water mixtures of 1 and 2 M DMSO and PG, respectively, during a cooling at 5 °C·min^{-1}.

Figure 8 depicts the change in V_c/V_c^{iso} of human corneal keratocytes after initially being exposed to DMSO−NaCl−water

dx.doi.org/10.1021/jp2054348 |J. Phys. Chem. B 2011, 115, 14721–14731

and PG−NaCl−water mixtures with CPA molalities of 1 and 2 M, respectively, during a 5 °C·min^{-1} freezing protocol. The curves $V_c/V_c^{iso} \sim T$ are calculated with eqs 28 and 29 and eqs 36 and 37, respectively. It is shown that the deviation of the dilute and ideal results from the real ones will be more obvious as the molality increases (i.e., as the solution becomes more nondilute and nonideal). Human corneal keratocytes will lose less water when they are exposed to the PG−NaCl−water mixture than when exposed to the DMSO−NaCl−water one. This is in part because k_w for PG is always smaller than that for DMSO at the same T. Since the water loss is less dramatic, the cellular change will be correspondingly less dramatic. Additionally, it is found that the difference between the solid and dashed lines for the PG−NaCl−water mixture is larger than that for the DMSO−NaCl−water one. This is mainly due to different physical and chemical properties of PG and DMSO.

4. CONCLUSIONS

Most of thermodynamic and kinetic models in cryobiology focus primarily on dilute and ideal solutions. More importantly, the current nonisothermal models failed to couple the transmembrane transport of water and permeable CPAs when cells are subjected to various temperature profiles. To overcome these deficiencies, this study develops a new set of nondilute and nonideal equations that are able to calculate the transport of both water and permeable CPA of cells during the freezing and thawing protocols. Our new models can also be simplified into the formalisms in the literature by including certain assumptions. Specifically, eqs 12 and 15 are equations of the dilute and ideal nonisothermal 2-P model, while eqs 28 and 29 comprise the nondilute and nonideal nonisothermal 2-P one. The comparisons given by our new models and their applications to the cryopreservation of ICR mouse spermatozoa and human corneal keratocytes will expand our knowledge of the physical response of biological cells during cryopreservation.

AUTHOR INFORMATION

Corresponding Author

*Tel.: +86-411-84708774. Fax: +86-411-84708460. E-mail: wzhongli@dlut.edu.cn.

ACKNOWLEDGMENT

The support from the National Nature Science Foundation of China (50976017) and NSFC's Key Program Projects (50736001) is greatly appreciated.

REFERENCES

(1) Polge, C.; Smith, A. U.; Parkes, A. S. *Nature* **1949**, *164*, 666.
(2) Mazur, P. *Cryobiology* **2010**, *60*, 4–10.
(3) Jacobs, M. H. *J. Cell. Comp. Physiol.* **1933**, *2*, 427–444.
(4) Jacobs, M. H.; Stewart, D. R. *J. Cell. Comp. Physiol.* **1932**, *1*, 71–82.
(5) Kedem, O.; Katchalsky, A. *Biochim. Biophys. Acta* **1958**, *27*, 229–246.
(6) Onsager, L. *Phys. Rev.* **1931**, *37*, 405–426.
(7) Onsager, L. *Phys. Rev.* **1931**, *38*, 2265–2279.
(8) Kleinhans, F. W. *Cryobiology* **1998**, *37*, 271–289.
(9) Elmoazzen, H. Y.; Elliott, J. A. W.; McGann, L. E. *Biophys. J.* **2009**, *96*, 2559–2571.
(10) Katkov, I. I. *Cryobiology* **2000**, *40*, 64–83.
(11) Mazur, P. *J. Gen. Physiol.* **1963**, *47*, 347–369.
(12) Karlsson, J. O. M.; Cravalho, E. G.; Toner, M. *J. Appl. Phys.* **1994**, *75*, 4442–4455.
(13) Fahy, G. M. *Cryobiology* **1981**, *18*, 473–482.
(14) Weng, L.; Li, W.; Zuo, J. *Cryobiology* **2010**, *61*, 194–203.
(15) Saenz, J.; Toner, M.; Risco, R. *J. Phys. Chem. B* **2009**, *113*, 4853–4864.
(16) Prickett, R. C.; Elliott, J. A. W.; McGann, L. E. *Cryobiology* **2010**, *60*, 30–42.
(17) Abazari, A.; Elliott, J. A. W.; Law, G. K.; McGann, L. E.; Jomha, N. M. *Biophys. J.* **2009**, *97*, 3054–3064.
(18) Prickett, R. C.; Elliott, J. A. W.; Hakda, S.; McGann, L. E. *Cryobiology* **2008**, *57*, 130–136.
(19) Elliott, J. A. W.; Prickett, R. C.; Elmoazzen, H. Y.; Porter, K. R.; McGann, L. E. *J. Phys. Chem. B* **2007**, *111*, 1775–1785.
(20) Ross-Rodriguez, L. U.; Elliott, J. A. W.; McGann, L. E. *Cryobiology* **2010**, *61*, 46–51.
(21) Ross-Rodriguez, L. U.; Elliott, J. A. W.; McGann, L. E. *Cryobiology* **2010**, *61*, 38–45.
(22) Mukherjee, I. N.; Li, Y.; Song, Y. C.; Long, R. C., Jr; Sambanis, A. *Osteoarthritis Cartilage* **2008**, *16*, 1379–1386.
(23) Agre, P.; Kozono, D. *FEBS Lett.* **2003**, *555*, 72–78.
(24) Smith, B. L.; Agre, P. *J. Biol. Chem.* **1991**, *266*, 6407–6415.
(25) Denker, B. M.; Smith, B. L.; Kuhajda, F. P.; Agre, P. *J. Biol. Chem.* **1988**, *263*, 15634–15642.
(26) Mortimer, R. G. *Physical Chemistry*; Academic Press: New York, 2008.
(27) Kleinhans, F. W.; Mazur, P. *Cryobiology* **2007**, *54*, 212–222.
(28) Weng, L.; Li, W.; Zuo, J. *Thermochim. Acta* **2011**, *512*, 225–232.
(29) Han, X.; Liu, Y.; Critser, J. K. *Cryobiology* **2010**, *61*, 52–57.
(30) Pegg, D. E. *Cryo Lett.* **1986**, *7*, 387–394.
(31) Devireddy, R. V.; Raha, D.; Bischof, J. C. *Cryobiology* **1998**, *36*, 124–155.
(32) Weng, L.; Li, W.; Zuo, J. *Cryobiology* **2011**, *62*, 210–217.
(33) Angell, C. A.; Sichina, W. J.; Oguni, M. *J. Phys. Chem.* **1982**, *86*, 998–1002.
(34) Giauque, W. F.; Stout, J. W. *J. Am. Chem. Soc.* **1936**, *58*, 1144–1150.
(35) Weng, L.; Li, W.; Zuo, J.; Chen, C. *J. Chem. Eng. Data* **2011**, *56*, 3175–3182.
(36) Phelps, M. J.; Liu, J.; Benson, J. D.; Willoughby, C. E.; Gilmore, J. A.; Critser, J. K. *Biol. Reprod.* **1999**, *61*, 1031–1041.
(37) Ebertz, S. L. Fundamental cryobiology of cells from a bioengineered human corneal equivalent. Ph.D. Thesis, University of Alberta, 2002.
(38) Ebertz, S. L.; McGann, L. E. *Cryobiology* **2004**, *49*, 169–180.
(39) Devireddy, R. V.; Swanlund, D. J.; Roberts, K. P.; Bischof, J. C. *Biol. Reprod.* **1999**, *61*, 764–775.